Cell

Self-Organized Shuttling: Generating Sharp Dorsoventral Polarity in the Early *Drosophila* Embryo

Michal Haskel-Ittah,[1] Danny Ben-Zvi,[1] Merav Branski-Arieli,[1] Eyal D. Schejter,[1] Ben-Zion Shilo,[1,*] and Naama Barkai[1,*]
[1]Department of Molecular Genetics, Weizmann Institute of Science, Rehovot 76100, Israel
*Correspondence: benny.shilo@weizmann.ac.il (B.-Z.S.), naama.barkai@weizmann.ac.il (N.B.)
http://dx.doi.org/10.1016/j.cell.2012.06.044

SUMMARY

Morphogen gradients pattern tissues and organs during development. When morphogen production is spatially restricted, diffusion and degradation are sufficient to generate sharp concentration gradients. It is less clear how sharp gradients can arise within the source of a broadly expressed morphogen. A recent solution relies on localized production of an inhibitor outside the domain of morphogen production, which effectively redistributes (shuttles) and concentrates the morphogen within its expression domain. Here, we study how a sharp gradient is established without a localized inhibitor, focusing on early dorsoventral patterning of the *Drosophila* embryo, where an active ligand and its inhibitor are concomitantly generated in a broad ventral domain. Using theory and experiments, we show that a sharp Toll activation gradient is produced through "self-organized shuttling," which dynamically relocalizes inhibitor production to lateral regions, followed by inhibitor-dependent ventral shuttling of the activating ligand Spätzle. Shuttling may represent a general paradigm for patterning early embryos.

INTRODUCTION

Morphogens are signaling molecules that can induce several cell fates in a concentration-dependent manner (Wolpert, 1989). Gradients of morphogens are instrumental in patterning tissues and organs during the development of multicellular organisms, raising interest in the molecular networks establishing these gradients. In the standard paradigm, a morphogen that is secreted from a localized source establishes a gradient that peaks at the source merely by its diffusion and degradation across the field. Quantitative properties of such gradients are well understood: morphogen spread is defined by the diffusion and degradation rates, and the sensitivity of the gradient to perturbations can be tuned by feedbacks acting on these parameters (Bollenbach et al., 2005; Eldar et al., 2003; Paulsen et al., 2011; Schier, 2009).

Classical examples of morphogen gradients conform to this paradigm, including the Bicoid and Dpp gradients in the *Drosophila* embryo (Driever and Nüsslein-Volhard, 1988a, 1988b; Ephrussi and St Johnston, 2004) and wing imaginal disc (Cadigan, 2002; Lecuit et al., 1996; Nellen et al., 1996), respectively. However, there are also examples where a morphogen is uniformly produced within a wide region, but its graded signaling is confined to a narrow domain that is well within the region of morphogen production. This paradigm is prevalent at early stages of embryogenesis, where broad domains have been defined, but the narrow territory responsible for local production of graded signals has not yet been generated. Quantitative properties of such gradients are less understood. Of particular interest are mechanisms that enable the generation of a sharp gradient and maintain its distribution robust to fluctuations in gene dosages or environmental conditions.

Previously, we analyzed this paradigm of a broadly expressed morphogen in the context of the BMP activation gradient in the early *Drosophila* embryo, which is formed well within the domain in which the activating ligand, Dpp, is expressed (dorsal ~40% of the embryo) (Eldar et al., 2002). Formation of the BMP activation gradient relies on the production of an inhibitor molecule (Sog) in regions flanking the dorsal domain where Dpp is produced. Sog is secreted, diffuses into the dorsal domain, and generates an inhibition gradient. Work by us and others described a novel shuttling mechanism for the formation of this activation gradient: rather than passively inhibiting BMP signaling, the diffusible flux of Sog serves to redistribute the Dpp molecules, concentrating the ligand in the dorsal-most region (Eldar et al., 2002; Mizutani et al., 2005; Shimmi et al., 2005; Wang and Ferguson, 2005).

Theoretical analysis suggested that shuttling provides two advantages: first, it leads to a sharp gradient; second, it enhances the robustness of the gradient to fluctuations in gene dosage (Eldar et al., 2002; Meinhardt and Roth, 2002). The shuttling mechanism is conserved in short-germband insects (van der Zee et al., 2006), and we recently provided evidence that shuttling functions also in the early *Xenopus* embryo, again in generating a BMP activation gradient (Ben-Zvi et al., 2008; Plouhinec et al., 2011). Notably, redistribution of ligand molecules via shuttling does not involve directed transport but depends only on nondirected diffusion.

In the aforementioned example of the BMP activation gradient, expression of an inhibitor outside the patterned domain serves as the key asymmetry cue and is the critical factor in generating a sharp and robust gradient through ligand shuttling.

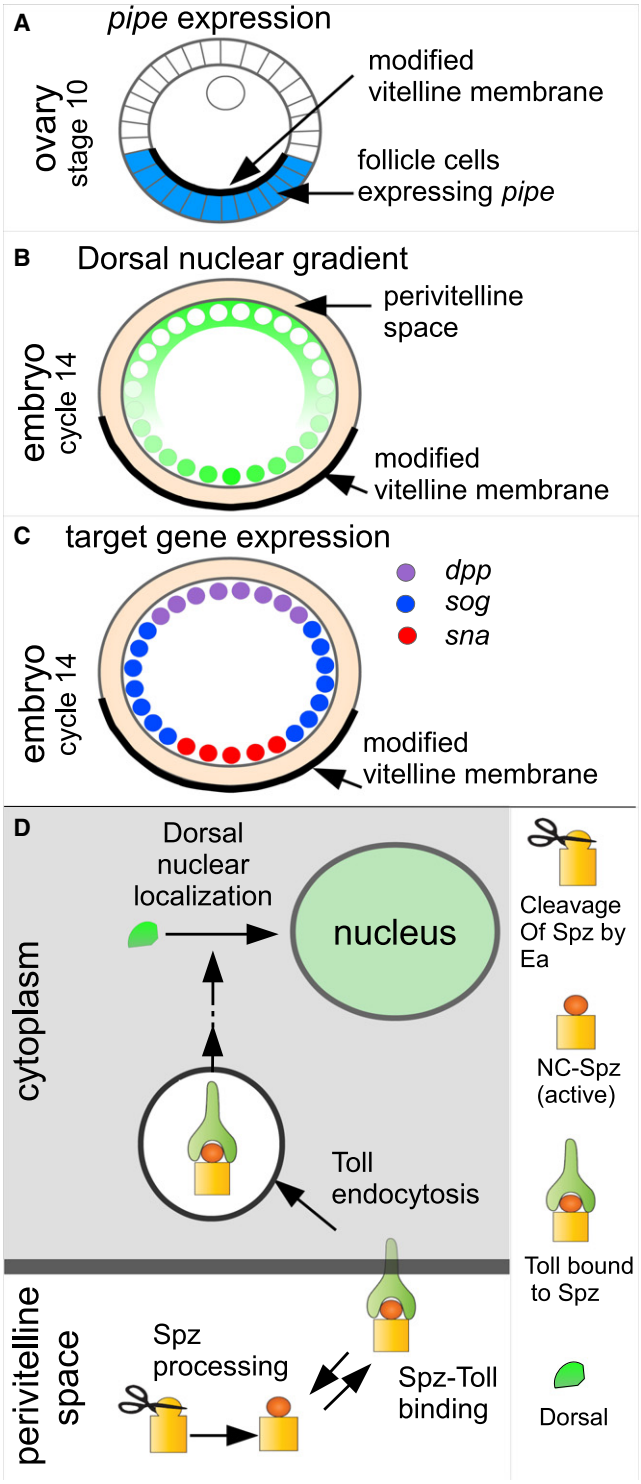

Figure 1. DV Axis Formation in *Drosophila*: From Ovary to Embryo

(A) A schematic cross-section of a stage 10 ovary: *pipe* expression (blue) in the follicular epithelium is restricted to a uniform ventral domain occupying 40% of the ventralmost cells. Pipe leads to the modification of the vitelline membrane (black), which surrounds the late oocyte and early embryo.

(B and C) Schematic cross-section of an early embryo. (B) A gradient of nuclear Dl (an NFκB transcription factor) is established peaking in the ventral midline.

(C) Dl regulates the expression of zygotic genes that determine cell fates along the DV axis in the embryo. High nuclear concentration of Dl activates the transcription of *sna* (red, confined to ~20% ventral region), whereas intermediate and low nuclear Dl induce *sog* (blue). *dpp* (purple) is found in cells lacking nuclear Dl.

(D) Ea, a serine protease present in the perivitelline fluid surrounding the embryo is processed and activated in the ~40% ventral region defined by *pipe* expression. Activated Ea cleaves Spz, an NGF-like ligand, to form the ligand NC-Spz. NC-Spz binds Tl receptor and thus triggers the nuclear localization of Dl.

Yet in other cases, such asymmetry may not exist, and gradient formation within the broad expression domain will need to be established without the assistance of external cues. We wished to examine how a sharp gradient is established in these cases and whether similar principles apply.

The transmission of dorsoventral (DV) polarity from the *Drosophila* oocyte to the embryo is a case in point (Moussian and Roth, 2005). During oogenesis, the ventral 40% of the follicle cell layer surrounding the oocyte is patterned by the EGF receptor pathway to express the gene *pipe*, encoding a sulfotransferase (Anderson, 1998; James et al., 2002; Morisato and Anderson, 1995; Peri et al., 2002; Sen et al., 1998; Stein, 1995). Modification by Pipe is thought to activate proteins, which are deposited on the vitelline membrane covering the oocyte and the future embryo (Sen et al., 1998; Zhang et al., 2009; Zhu et al., 2007). Following fertilization, the ventral domain of the vitelline membrane, which was defined by *pipe* expression, guides the subsequent polarity of the embryo by facilitating a proteolytic cascade within the perivitelline space (Figure 1), which culminates in the processing and activation of Spätzle (Spz), a ligand of the Toll (Tl) receptor (Cho et al., 2012; DeLotto and DeLotto, 1998; DeLotto et al., 2001; Dissing et al., 2001; LeMosy et al., 1999; Morisato and Anderson, 1994; Schneider et al., 1994; Weber et al., 2003).

Binding of processed Spz to the Tl receptor on the embryonic plasma membrane activates a signaling pathway within the embryo, whose outcome is the graded nuclear localization of the transcription factor Dorsal (Dl) within embryonic nuclei (Roth et al., 1989; Rushlow et al., 1989; Stathopoulos and Levine, 2002). Notably, this ventral-to-dorsal gradient is generated well within the *pipe* domain. Thus, whereas *pipe* is found uniformly along the ventral 40% of the egg chamber, Dl appears fully nuclear in less than 20% of the circumference and becomes progressively cytoplasmic dorsally. Moreover, gene expression boundaries, such as those defining the expression domains of the high-Dl target genes *twist* (*twi*) and *snail* (*sna*), are also found at the ventral ~20% (Rusch and Levine, 1996; Stathopoulos and Levine, 2002; Zhao et al., 2007). Evidence further suggests that elaboration of the wide *pipe* domain into a narrower gradient of Tl activation involves a self-organization circuit because expanding the *pipe* domain to ~80% of the follicle cells results in a two-peak gradient (Morisato, 2001; Moussian and Roth, 2005; Roth and Schüpbach, 1994). However, how this self-organization is encoded by the molecular machinery remains unknown.

We searched computationally for mechanisms that can generate a sharp and robust gradient within the expression

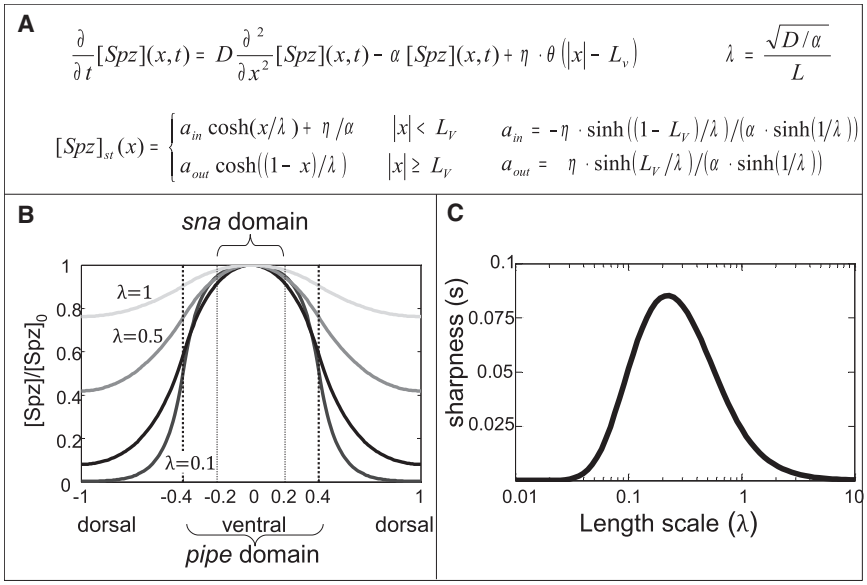

Figure 2. Morphogen Diffusion Generates a Shallow Gradient within the Source

(A) The equation defining the naive reaction-diffusion model and its steady-state solution. *[Spz](x,t)* denotes the concentration of Spz in space and time, *D* is the diffusion coefficient, α the Spz degradation rate, and η the rate by which Spz is produced, which is restricted to L_v, the 40% ventral domain. λ is the length scale defining this system. cosh and sinh are the hyperbolic cosine and hyperbolic sine, accordingly.

(B) Steady-state profiles of activated Spz for different values of λ, as indicated. The profiles are normalized by their maximum value at x = 0. *pipe* and *sna* expression domains are indicated by the broken and solid vertical lines, respectively. x = 0 represents the ventral midline.

(C) The sharpness of Spz profile as a function of λ. The sharpness is defined as the relative change in concentration between the maximal value (at x = 0) and the value at the *sna* border (x = 0.2).

See also Figure S1.

domain of a broadly produced ligand. We show that a simple model, which relies only on the diffusion of the ligand outside its expression domain, does not suffice. Based on reported properties of the Spz ligand (DeLotto and DeLotto, 1998; DeLotto et al., 2001; Morisato, 2001; Weber et al., 2003), we consider the case where the diffusing morphogen is cleaved to generate an inhibitor that can either inhibit ligand activity or compete for receptor binding. This scenario, however, does not suffice for sharpening the gradient. Rather, we again identify an inhibitor-mediated shuttling mechanism as a way for producing a sharp and robust gradient. Notably, in this case the inhibitor is not produced outside the domain of morphogen expression but, instead, is generated concomitantly with the ligand following its cleavage. Shuttling emerges as a self-organized property of the dynamics, with polar inhibitor production established in a self-consistent manner. Key assumptions of this model are based on known biochemical properties of Spz cleavage (Weber et al., 2007), and we demonstrate the consistency of the mechanism with published genetic experiments, including the observed formation of a double peak when the *pipe* expression domain is expanded. We further provide experimental evidence demonstrating multiple facets of the ligand Spz following cleavage and the capacity to polarize the DV axis according to the flux of the inhibitory Spz prodomain, all consistent with use of shuttling by the early DV patterning network.

RESULTS

Computational Model: Searching for a Mechanism that Establishes a Sharp and Robust Morphogen Gradient

We consider a morphogen that is produced in a wide region and examine the gradient of morphogen level that is established within this domain of expression. As a concrete case, we assume the morphogen production domain is restricted to 40% of the embryonic circumference, matching the observed extent of the *pipe* domain where activated Spz is produced (Peri et al., 2002). In addition, the first gene expression boundary is established at 20% circumference, matching the expression boundary of the Dl target gene *sna*. Recent measurements of the Dl gradient have shown that the gradient decays by almost 50% over this 20% spatial range (Kanodia et al., 2009; Liberman et al., 2009; Stathopoulos and Levine, 2002). To rigorously define the steepness of the gradient ("sharpness"), we measure the relative decay from its maximal level, found at x = 0, to its value at the expression boundary, $x = L_V/2$, L_V being the size of the morphogen expression domain, with embryo size normalized to 1.

Spz, the Tl-activating ligand, is uniformly processed by proteolytic cleavage throughout the *pipe* domain. The Spz precursor can be cleaved to generate two entities: the C-terminal domain (C-Spz), which functions as an activating ligand (DeLotto et al., 2001; Weber et al., 2003); and an N-terminal domain (N-Spz), whose overexpression inhibits ventral fates (Morisato, 2001). The mere diffusion of the activated C-Spz away from the domain of morphogen production could produce a gradient within the production domain. However, we noted that such diffusion produced a very shallow gradient (Figures 2A–2C). In fact, analytical analysis confirmed that the maximal sharpness that can be achieved by diffusion of C-Spz out of its domain of expression is 9%, a value that renders the gradient highly sensitive to even small fluctuations in the production or degradation rates of the morphogen, and cannot be used to support robust patterning. Furthermore, extending the model to include nonlinear degradation of Spz did not increase the sharpness of the gradient (Figure S1 available online). Similarly, adding cogeneration of the inhibitory N-Spz and activating C-Spz was not sufficient for producing a sharp gradient (Extended Experimental Procedures).

A Self-Organized Shuttling Mechanism Produces a Sharp and Robust Gradient

We considered the recently reported observation that following cleavage of the Spz precursor by the serine protease Easter (Ea), the separate C- and N-terminal parts of Spz remain

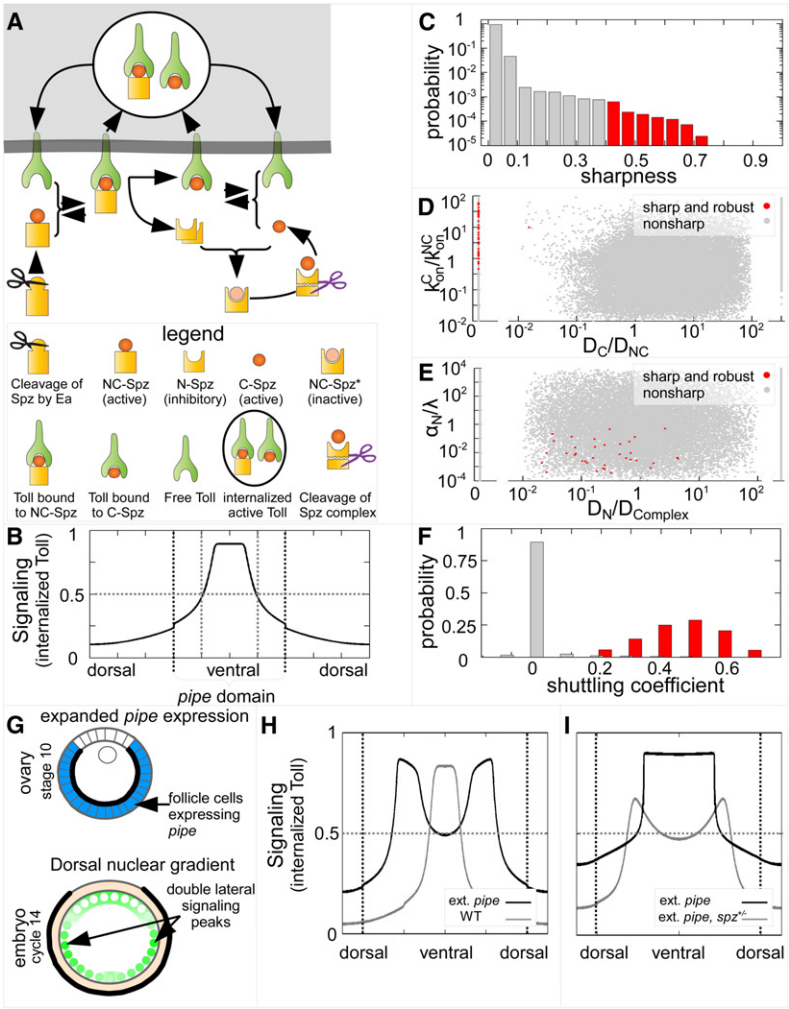

Figure 3. Formation of a Sharp Gradient by Self-Organized Shuttling

(A) Molecular model is shown. Cleavage of Spz by Ea produces an active ligand, NC-Spz. Binding of NC-Spz to the receptor Tl may lead to either internalization of the active ligand-receptor complex, or to its dissociation into two inhibitory molecules of N-Spz and an active complex of Tl bound to C-Spz. This complex, in turn, may internalize or dissociate into a free receptor and a free active ligand, C-Spz. C-Spz and N-Spz can bind to form an inert complex, NC-Spz*, which can be cleaved in the *pipe* domain, releasing C-Spz while degrading or inactivating N-Spz. Internalized receptors are the molecular signaling species. Receptors are recycled, whereas internalized ligands are degraded.

(B–F) Numerical screen is shown. A numerical screen was run on the kinetic parameters defining the interactions in (A), allowing also the diffusion and turnover of molecular species, to find parameters that result in sharp and robust signaling profiles (Experimental Procedures).

(B) Particular screen result. A signaling profile (levels of internalized Tl) exhibiting a sharp decrease from the ventral midpoint to the border of *sna* expression (gray vertical dashed lines). *pipe* expression domain is marked with heavy dashed lines. The threshold for *sna* expression is set to half of the maximal signaling level (gray horizontal dashed line).

(C) About one million parameter sets were tested, and only 0.04% were found to be consistent sets, forming a sharp (sharpness >0.4) profile that is robust to parameter perturbations. Over 99% of the solutions had sharpness smaller than 0.1.

(D and E) Consistent parameter sets, in red, were characterized by effectively no diffusion of C-Spz, and faster binding dynamics of C-Spz to Tl than NC-Spz to Tl (D). N-Spz was degraded much faster when in complex with C-Spz, and diffused slower than the inert NC-Spz* complex. Note that almost all consistent parameter sets (red) display no diffusion of C-Spz (E). Gray dots in (D) and (E) represent biologically valid but nonsharp gradients (Extended Experimental Procedures).

(F) Sharp and robust solutions are characterized by shuttling of C-Spz ventrally from its ventro-lateral production domain. Although most solutions displayed almost no shuttling, sharp and robust solutions had a positive shuttling coefficient. To achieve better statistics, a subsequent screen was run to identify over 3,000 parameter sets resulting in shuttling, using parameter characterization in (D) and (E). See Extended Experimental Procedures for definition of the shuttling parameter.

(G) Expanding the *pipe* expression domain to the ventral 80% of the ovary may result in double lateral peaks of Dl nuclear localization in the embryo.

(H) Parameter sets resulting in a sharp and robust gradient (gray) may form a double signaling peak (black) when the *pipe* expression domain is expanded to the ventral 80% of the ovary (ext. *pipe*). Black dashed lines denote the extended *pipe* expression domain; gray dashed line denotes the threshold for *sna* expression.

(I) In accordance with experimental results, some consistent sets display an expanded ventral signaling peak (ext. *pipe*, black). Reducing the *spz* gene dosage reveals the double signaling peak (ext. *pipe*, $spz^{+/-}$, gray). Markings as in (H).

See also Figure S2 and Tables S3 and S4.

associated (Weber et al., 2007). This form of the Spz ligand (NC-Spz) can bind and activate the Tl receptor (Figure 3A). Binding to the Tl receptor is in fact necessary for the final dissociation of the C- and N-terminal parts, generating a free activator (C-Spz) and inhibitor (N-Spz). We reasoned that this property might provide additional regulation of inhibitor production and may sharpen the gradient.

We formulated a mathematical model that accounts for this two-step process of free ligand production. The model allows for the rebinding of the dissociated N- and C-Spz portions to produce an inactive complex (NC-Spz*), and considers the endocytosis of Tl following activation (Lund et al., 2010), which is taken as a measure for signaling. A general analytical solution is not available, and we therefore studied the dynamics of the model using numerical simulations. Specifically, we searched systematically for parameters such as kinetic rate constants and diffusion rates, for which a sharp and robust activation gradient is established.

Although most parameters define a gradient that is rather shallow within the *pipe region* ($x < L_V$), sharp and robust

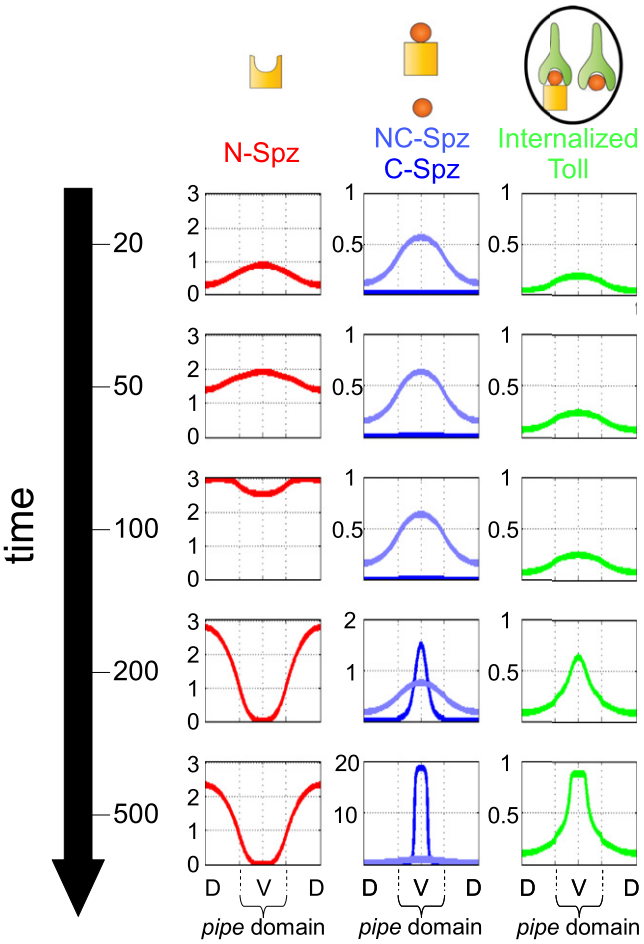

Figure 4. Dynamics of Gradient Formation Reveals Self-Organized Shuttling

Shown are the spatial profiles of the inhibitor, N-Spz (red), the active ligands NC-Spz (light blue) and C-Spz (blue), and the internalized Tl levels (green) in time from early (top) to late (bottom). The signaling gradient is initially dominated by NC-Spz, forming a shallow gradient defined by diffusion. N-Spz accumulates following binding of NC-Spz to Tl. Formation of the inert complex with C-Spz and the subsequent degradation of the complex in the ventral domain leads to a dip in N-Spz levels in the lateral domain. A ventral flux of N-Spz facilitates shuttling and leads to the formation of a sharp C-Spz gradient and further polarization of N-Spz gradient. In the ventral domain of the signaling gradient, the internalized receptor, becomes gradually dominated by C-Spz, whereas the dorsal and lateral domains are mostly affected by NC-Spz. Note the change of scale in the middle row. See also Figure S3 and Tables S1, S2, S4, and S5.

gradients did emerge (Figures 3B and 3C). This is in marked contrast to models that considered an immediate, one-step separation between N- and C-Spz following cleavage by Ea, where no sharp gradients could be identified (Extended Experimental Procedures). The sharp solutions were confined to a subset of the parameter space with several characteristics. First, C-Spz did not diffuse freely. Rather it diffused only in association with N-Spz, in either the active (NC-Spz) or inactive (NC-Spz*) complexes. Second, the binding and dissociation kinetics between NC-Spz and the Tl receptor were slower than that of the free C-Spz (Figure 3D; note that in all simulations, the dissociation constant [ratio of on versus off rate] was kept the same, in accordance with experimental results by Weber et al., 2007).

Inactivation of N-Spz is an important additional feature. In all consistent solutions, N-Spz was inactivated mostly while in complex with C-Spz, and this inactivation was biased toward the ventral domain defined by *pipe* expression (Figure 3E). One plausible mechanism may involve a protease that cleaves N-Spz in the NC-Spz* complex, to release active C-Spz. Interestingly, a Pipe-dependent mechanism by which Gastrulation defective (GD) ventrally restricts the processing of Ea by Snake (Snk) was recently reported by Cho et al. (2012). This suggests that the protease that carries out the putative cleavage of the inactive complex could potentially be Ea or Snk.

The Dynamic Formation of a Sharp Gradient through Self-Organized Shuttling

Examining the consistent solutions that produced a sharp gradient, we noticed that in all cases, the active ligand C-Spz was concentrated toward the ventral midline, $x = 0$. Thus, the sharp gradient was produced not merely by a graded inhibition of a uniformly produced ligand but by the physical translocation of the ligand toward the center from a broad production domain (Figure 3F; Extended Experimental Procedures). As described above, this is the hallmark of a shuttling mechanism (Eldar et al., 2002; Meinhardt and Roth, 2002). Furthermore, several of the biochemical properties characterizing the consistent solutions are defining properties of the canonical shuttling mechanism: low diffusion of the active ligand C-Spz, facilitation of C-Spz movement by binding to the inhibitor N-Spz, and the enhanced degradation of N-Spz when in complex with C-Spz (Figures 3D and 3E).

Identifying the shuttling mechanism here was surprising to us because shuttling of the ligand by its inhibitor is possible only when there is a flux of inhibitor toward the center. Here, however, Spz is processed within the entire *pipe* domain. Moreover, the inhibitor is produced following the binding of the processed ligand (NC-Spz) to the receptor, which is expected to occur primarily throughout the ventral *pipe* expression domain. What then leads to a polarized production of the inhibitor?

Examining the dynamics of gradient formation (Figure 4), we noted that initially, the signaling gradient is dominated by the processed ligand (NC-Spz), whose distribution is determined according to the simple diffusion model. However, binding of NC-Spz to Tl generates N- and C-Spz, mostly in the *pipe* domain. Rebinding of N- and C-Spz generates the inert complex (NC-Spz*) that is subsequently degraded in the *pipe* domain, causing effective degradation of N-Spz in the ventral part of the embryo, whereas C-Spz does not diffuse and is deposited ventrally. Ventral depletion of N-Spz leads to its accumulation laterally, outside the *pipe* domain. The ventral accumulation of C-Spz leads to occupation of the receptors by C-Spz in this domain. NC-Spz therefore binds Tl more laterally, releasing N-Spz in a polarized manner and leading to shuttling (animated in PaperFlick). The gradient can be divided into two regions. The ventralmost part is formed through shuttling and dominated by C-Spz. The sharp profile in this region is characteristic of the shuttling mechanism. The ventro-lateral domain is much flatter

because it is formed through diffusion of NC-Spz and dominated by this ligand. Interestingly, this division of the DV axis and the dynamics of the Dl nuclear gradient were recently observed experimentally by Reeves et al. (2012).

Reassociation between the Two Parts of Spz

Reassociation between N-Spz and C-Spz plays a crucial role in the model because it provides the means to shuttle C-Spz ventrally. To experimentally demonstrate that N-Spz and C-Spz possess the capacity to physically associate, we made use of two constructs: V5-tagged N-Spz fused C terminally to a transmembrane domain (V5-N-Spz-TM), and a secreted and biologically active signal peptide-C-Spz-GFP fusion protein (SP-C-Spz-GFP) (Figure 5A) (Cho et al., 2010). HeLa cells expressing membrane-anchored V5-N-Spz-TM were incubated with medium secreted by *Drosophila* S2 cells that had been transfected either with SP-C-Spz-GFP, or with a signal peptide-GFP (SP-GFP) fusion protein, that served as a control. Incubation and washes of the medium were carried out under conditions where endocytosis is inhibited, and the subsequent immunohistochemical staining was performed on nonpermeabilized cells, so that only extracellular proteins were detected. A strong GFP signal was displayed on most cells expressing N-Spz-TM and incubated with secreted SP-C-Spz-GFP (75%), but no such signal could be detected following incubation with the control medium (Figures 5B and 5C). These observations imply that, as predicted by the model, N- and C-Spz can readily reassociate.

The Reassociated N- and C-Spz Complex Is Inactive

A second prediction of the model is that the complex generated by reassociated N- and C-Spz (NC-Spz*) is inactive and is, therefore, functionally distinct from the biologically active NC-Spz, formed immediately after cleavage by Ea. To validate this prediction, we sought to test the activity of the reassociated complex in *Drosophila* embryos. We initially examined alterations in DV fates, following separate overexpression of N- and C-Spz, under control of the maternal driver *nos-Gal4*. Expression of SP-C-Spz-GFP in this manner led to a pronounced lateralizing effect. Although the ventralmost mesodermal fates and their position were not significantly altered, the expression domain of the lateral marker *intermediate neuroblasts defective* (*ind*) expanded considerably, to cover the entire dorsal side of the embryo, whereas dorsal fates, normally marked by expression of *dpp*, were strongly diminished. In contrast, expression of N-Spz by the same driver did not give rise to any detectable phenotype at the level of altered gene expression or cuticle patterns, and the embryos were viable.

A marked inhibitory effect of N-Spz was detected, however, following coexpression with SP-C-Spz-GFP. The expanded *ind* expression induced by SP-C-Spz-GFP was no longer apparent, and dorsal *dpp* expression was restored (Figures 5D–5L). These observations imply formation of a functionally distinct, reassociated complex between N- and C-Spz, which interferes with the capacity of C-Spz to activate the Tl signaling pathway. They further suggest that binding to C-Spz can account for the previously reported inhibitory activity of N-Spz when injected into early embryos (Morisato, 2001).

Interestingly, in the ventral region, coexpression of N- and C-Spz in this manner had an attenuating effect, such that the endogenous expression of ventro-lateral genes such as *ind* was abolished, and expression of the ventral marker *sna* became narrower. Because this effect was not observed upon expression of N-Spz alone (where the wild-type pattern was maintained), it represents an outcome of the reassociated N- and C-Spz complex. We hypothesize that this results from some interaction with other signaling processes that function in the ventral region, for example through interaction of the NC-Spz* with the Ea protease processing Spz, or by the formation of higher-order complexes between the N-Spz and C-Spz that inhibit Tl activation.

Self-Organized Shuttling Accounts for Axis Duplication

As an additional test of the model, we examined whether it can account for the observation that increasing the *pipe* expression domain from its endogenous 40% to 80% of the ventral region results in a pattern duplication: the monotonous single-peak gradient observed in wild-type is replaced by a two-peak profile in a significant portion of the embryos (Figure 3G) (Morisato, 2001; Moussian and Roth, 2005; Roth and Schüpbach, 1994). Indeed, we could readily identify parameters for which extending the region of Spz processing in the model leads to axis duplication (Figure 3I).

Notably, the resulting ventral minimum between the two peaks is rather shallow and may be close to the threshold value for *twi* and *sna* expression. This can explain why only half of the embryos showed axis duplication, whereas the rest showed an expanded *twi* expression domain (Morisato, 2001). Small differences in system parameters between different embryos can result in one embryo exhibiting a single, extended peak, and the other two peaks. The model can also explain the observation that reduction in *spz* gene dosage increases the fraction of embryos with two *twi* expression domains, in cases where the *pipe* expression domain was expanded (Morisato, 2001) (Figure 3H).

A simple explanation accounts for formation of the two peaks: shuttling is not sufficiently effective in concentrating the ligand at the midline but only to shift it from the edges of the *pipe* domain. As a result, the ligand is not concentrated toward the ventralmost regions, and signaling is below maximal levels.

The Phenotype of Uniform *pipe* Is Consistent with Self-Organized Shuttling

The double peak observed when the *pipe* domain is extended to 80% of the embryo was lost when *pipe* was expressed uniformly throughout the embryo (Sen et al., 1998). This is a surprising observation that presents a challenge to self-organized mechanisms that rely on the spontaneous breaking of symmetry, such as those described by a Turing mechanism (Turing, 1952). We asked if self-organized shuttling can account for this observation as well. Indeed, we find that when uniform cleavage of the Spz precursor is imposed on the model, no pattern is observed within the typical patterning time. Instead, the inability to concentrate the ligand toward the midline of the embryo predicts a uniform, intermediate level of signaling (Figures 6A and 6B; note that this symmetry can be broken, leading to a double-peak solution

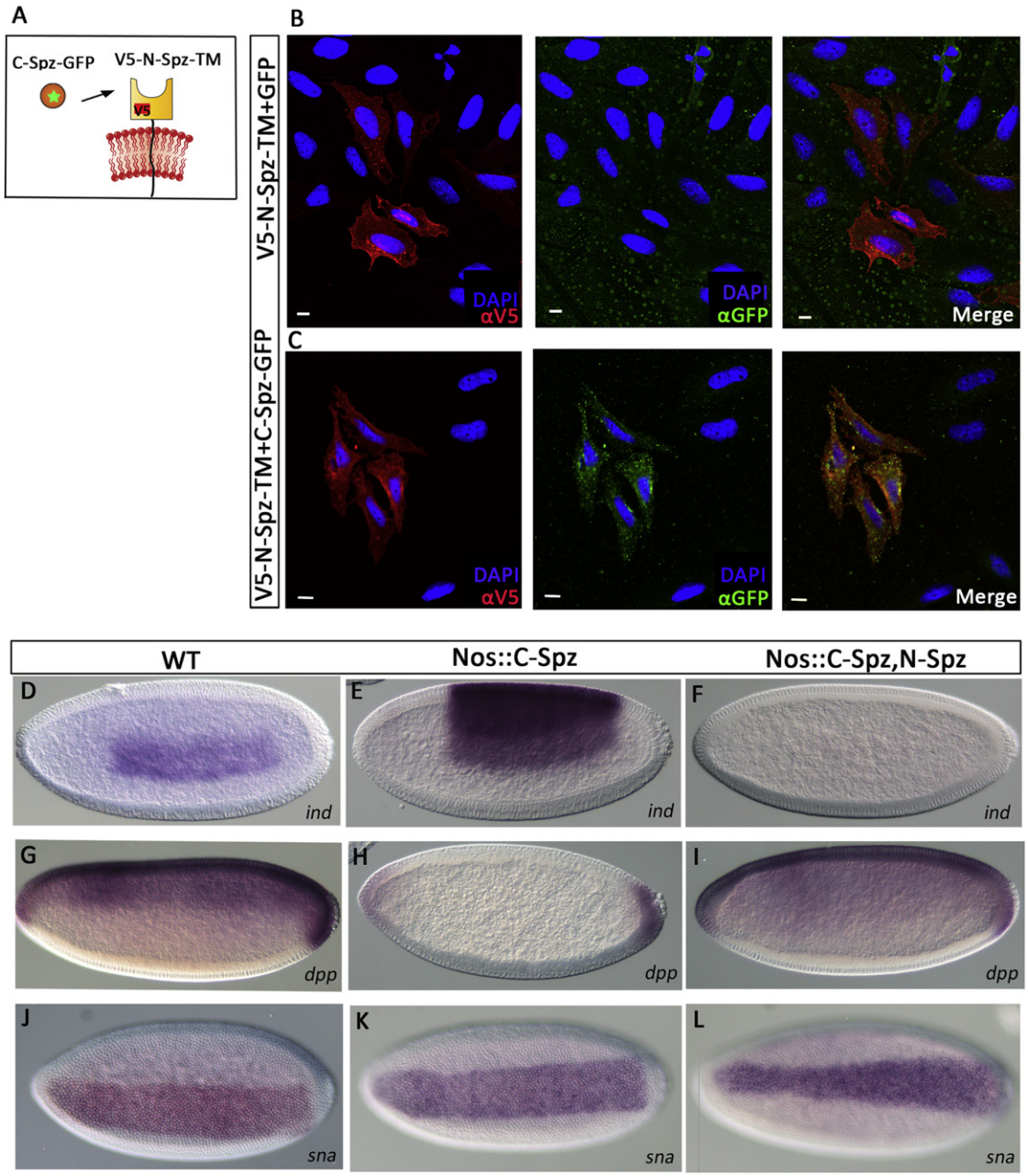

Figure 5. N-Spz and C-Spz Can Rebind and Create an Inactive Complex

(A) Schematic drawing of the experimental procedure: a membrane-anchored construct of N-Spz tagged with V5 was expressed in cells, and secreted C-Spz tagged with GFP was added to the medium.

(B) Secreted GFP (green) does not bind cells that are transfected with membrane-anchored N-Spz (red). Scale bars, 10 μm.

(C) C-Spz GFP (green) is attached specifically to cells that are transfected with membrane-anchored N-Spz (red). Scale bars, 10 μm.

(D, G, and J) RNA in situ hybridization to wild-type embryos with a probe to *ind*, *dpp*, and *sna*, respectively.

(E, H, and K) In embryos expressing *UAS-C-Spz* by *nos:Gal4* (E) *ind* expression is broader, (H) *dpp* expression is absent, and (K) *sna* expression is unaltered, indicating an elevation in Tl signaling in the dorsal region.

(F, I, and L) In embryos expressing *UAS-C-Spz* and *UAS-N-Spz* using *nos:Gal4*, (F) *ind* expression is absent, (I) *dpp* reappears, and (L) *sna* is mildly narrower, indicating an abolishment of the effects of ectopic C-Spz.

Anterior is oriented toward the left, and dorsal is up in (D)–(L).

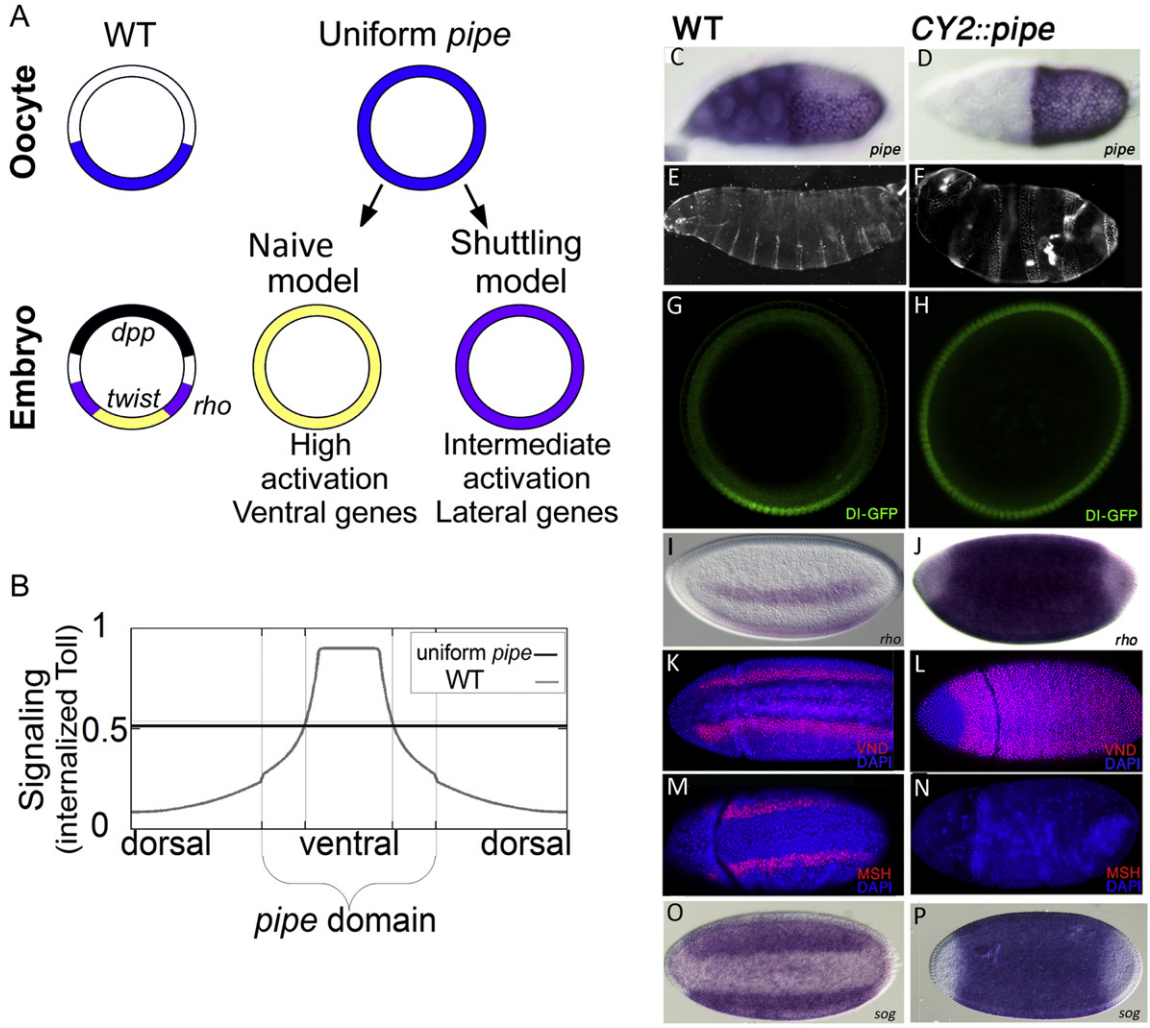

Figure 6. Uniform Expression of *pipe* Leads to Lateralization of the Embryo

(A) Predicted phenotype upon uniform *pipe* expression: naive models predict maximal Tl receptor activation leading to uniform *twi* and *sna* expression. In contrast the shuttling model predicts medium activation because the ligand is not concentrated ventrally, leading to lateral fates and the expression of ventro-lateral genes as *rho*.

(B) A uniform profile of activated Tl obtained upon uniform expression of *pipe.* The black curve is the numerical solution obtained when *pipe* is taken to be uniformly expressed in the follicular epithelium, and the gray curve is the profile of Tl activation obtained for the same parameters in the wild-type case. *sna* expression threshold is indicated by the dashed gray horizontal line.

(C–P) Experimental results supporting the shuttling model.

(C) Stage 10 ovary of a wild-type female stained by an RNA probe for *pipe*. *pipe* is expressed in the ventral 40% of the follicular epithelium.

(D) Stage 10 ovary of a *cy2:Gal4; UAS-pipe* female stained by the same probe. *pipe* is expressed uniformly in all the follicular epithelium. Note that WT *pipe* in situ detects also nurse cell staining because of the longer exposure, compared to the exposure time in the uniform *pipe* case (approximately six times longer). (E, G, I, K, M, and O) Progeny of WT females. (F, H, J, L, N, and P) Progeny of *cy2:Gal4; UAS-pipe* females.

(E) Lateral view of larval cuticle: stripes of ventral denticles are formed along the AP axis in the ventro-lateral region.

(F) Larval cuticles show the formation of rings of ventral denticle material, indicating acquisition of ventro-lateral fate throughout the DV axis.

(G and H) GFP staining of Dl-GFP in early stage 4 embryos laid by WT (G) and *cy2:Gal4; UAS-pipe* (H) females. In the WT case a gradient of nuclear Dl is observed with a peak in the ventral region. In the uniform *pipe* case, nuclear Dl is distributed uniformly in the nuclei, at an intermediate level corresponding to lateral fates.

(I and J) *rho* expression pattern in a stage 5 embryo laid by WT (I) and *cy2:Gal4; UAS-pipe* (J) females. In the WT case, *rho* is expressed in ventro-lateral stripes (the image was taken from a ventro-lateral view). In the uniform *pipe* case, *rho* displays a uniform expression along the DV axis (the image was taken from a lateral view).

(K and L) Ventral view of Vnd protein staining of early embryos laid by WT (K) and *cy2:Gal4; UAS-pipe* (L) females. Normally, Vnd is expressed in ventro-lateral stripes, but in the uniform *pipe* case, it is expressed uniformly throughout the embryo.

(M and N) Ventral view of Msh staining of early embryos laid by WT (M) and *cy2:GAL4; UAS-pipe* (N) females. In the WT case Msh is expressed in two lateral stripes, located dorsally to the Vnd stripes. In the uniform *pipe* case, Msh is not expressed at all.

(O and P) The expansion of ventro-lateral fates, following uniform expression of *pipe* in females, is also reflected by the expansion of the WT lateral *sog* expression domain (O) to the entire circumference of the embryo (P). These stainings reveal that the embryos laid by *cy2:Gal4; UAS-pipe* females acquire a ventro-lateral fate corresponding to the Vnd expression domain, throughout the DV axis.

See also Table S5.

following a delay that is significantly longer than the time in which the pattern is generated; data not shown).

This prediction of intermediate-level signaling in embryos following uniform expression of *pipe* during oogenesis is in fact a unique signature of shuttling, which requires the concentration of ligands in order to achieve maximal signaling levels. In contrast, mechanisms that rely only on the diffusion and degradation of C-Spz, and perhaps its inhibition by a coproduced inhibitor, naturally lead to a uniform, maximal level of activation throughout the embryo, when *pipe* is uniformly expressed.

Thus, our model predicts that uniform expression of *pipe* will lateralize, rather than ventralize, the embryos. Previous reports indicated that this is indeed the case. Embryos laid by females that express *pipe* uniformly in follicle cells lose any mark of polarity along the DV axis. Ventral gastrulation movements appear everywhere, and the larval cuticles show the formation of rings of denticle material, indicating lateralization of the progeny embryos (Sen et al., 1998).

To better define the precise degree of these fate shifts, we expressed *pipe* uniformly in follicle cells and followed both the expression of target genes and the nuclear localization of Dl in the embryo (Figures 6C–6P). The *rhomboid* (*rho*), *short gastrulation* (*sog*), and *ventral nervous system defective* (*vnd*) genes, which are normally expressed in the lateral neuroectoderm (Bier et al., 1990) or at a restricted domain within the neuroectoderm (Chu et al., 1998; McDonald et al., 1998), respectively, are seen throughout the circumference when *pipe* is uniform. A transgenic Dorsal-GFP (Dl-GFP), which faithfully recapitulates distribution of the Dl protein (DeLotto et al., 2007), shows a nuclear localization throughout the circumference at intermediate levels matching those of nuclei at the lateral region of wild-type embryos (Figures 6G and 6H). Together, these results indicate intermediate levels of Tl pathway activation throughout the embryo, consistent with the shuttling mechanism: despite the uniform activation of Spz resulting from ubiquitous *pipe* expression, maximal levels of Tl activation cannot be obtained in the absence of asymmetries and shuttling.

The Flux of N-Spz Dictates Mesoderm Position

The essence of the shuttling model is the redistribution of the active ligand by a shuttling molecule (N-Spz in this case), whose effective production domain flanks the morphogenic field. Upon association with the ligand, the shuttling molecule inhibits signaling. However, association provides the driving force for shuttling because the diffusion flux directs the release and concentration of the ligand in the region furthest from the region in which the shuttling molecule is produced. This distribution allows the shuttling molecule to function as an inhibitor of signaling close to the source that produces the shuttling molecule and as a facilitator of signaling furthest away from it.

To locally produce N-Spz, we capitalized on the fact that binding of NC-Spz to Tl promotes the dissociation between N- and C-Spz (Weber et al., 2007). A full-length Tl construct tagged C terminally with the Myc antigen was expressed at the anterior end of the embryo using the *Hsp83* maternal promoter and the *bcd* 3′ UTR. Staining for the Myc tag showed a highly restricted anterior localization (Figures 7A and S4), consistent with the limited diffusion capacity of Tl, even prior to cellularization (Huang et al., 1997).

Lateralized embryos display a uniform, intermediate level of Dl protein in all nuclei (Figure 7B). Expression of Toll-Myc (Tl-Myc) at the anterior end of such embryos alters the uniform nuclear distribution of Dl, affecting it in three major ways. First, high nuclear Dl levels are sometimes induced in the anterior region where Tl-Myc is expressed (Figure 7C). This local effect is likely to result from excess anterior expression of Tl and does not bear on our model. Second, the levels of nuclear Dl are diminished up to about half embryo length from the anterior pole, reflecting the shorter-range nonautonomous effect of releasing high levels of N-Spz, which can sequester and inactivate C-Spz (Figure 7D). Finally, the levels of nuclear Dl appear elevated toward the posterior pole, consistent with long-range facilitation of ligand release (Figure 7D).

To ascertain whether the shift to a nonuniform distribution of nuclear Dl following anterior Tl expression is reflected in the expression patterns of high nuclear Dl target genes, we monitored the *sna* mRNA pattern in lateralized embryos. A significant increase in the proportion of lateralized embryos expressing *sna*, following anteriorly localized expression of Tl-Myc, was indeed observed: from ~81% of lateralized embryos that did not express *sna* at all (Figure 7E) to ~59% *sna*-expressing embryos. In particular, 30% of the anterior-Tl-expressing embryos displayed a prominent posterior *sna* stripe (Figure 7G). Only 6% of embryos derived from females expressing *pipe* uniformly, but not anterior Tl, display this pattern (Figure 7F), a feature that can be attributed to rare, spontaneous symmetry breaking, which is in fact predicted by the model. Taken together, the changes in the patterns of Dl nuclear localization and *sna* gene expression upon anteriorly localized expression of Tl-Myc suggest that a flux of N-Spz can generate maximal signaling levels at the position that is furthest from its source.

Thus, ectopic expression of Tl at the anterior-most region establishes a signaling gradient along the anterior-posterior axis. This supports the main prediction of the shuttling mechanism: namely, the capacity of N-Spz to act as a nonautonomous short-range inhibitor and long-range activator of signaling.

DISCUSSION

A Self-Organized Shuttling Mechanism

By its nature, diffusion tends to homogenize concentration differences and is, therefore, not ideal for refining a wide expression domain into narrower gradients. Indeed, passive diffusion of a morphogen away from its source is insufficient for producing a sharp gradient within the source itself, as we demonstrated here. Yet, during early development, pattern often has to be established within a wide domain in which the morphogen is expressed.

We describe a self-organized shuttling mechanism that establishes a robust and sharp gradient of morphogen concentration within a broad domain of morphogen production in the early *Drosophila* embryo. This mechanism relies only on diffusion but necessitates an additional inhibitor molecule, which binds the morphogen and facilitates its diffusion. We and others have previously characterized the shuttling mechanism in the context

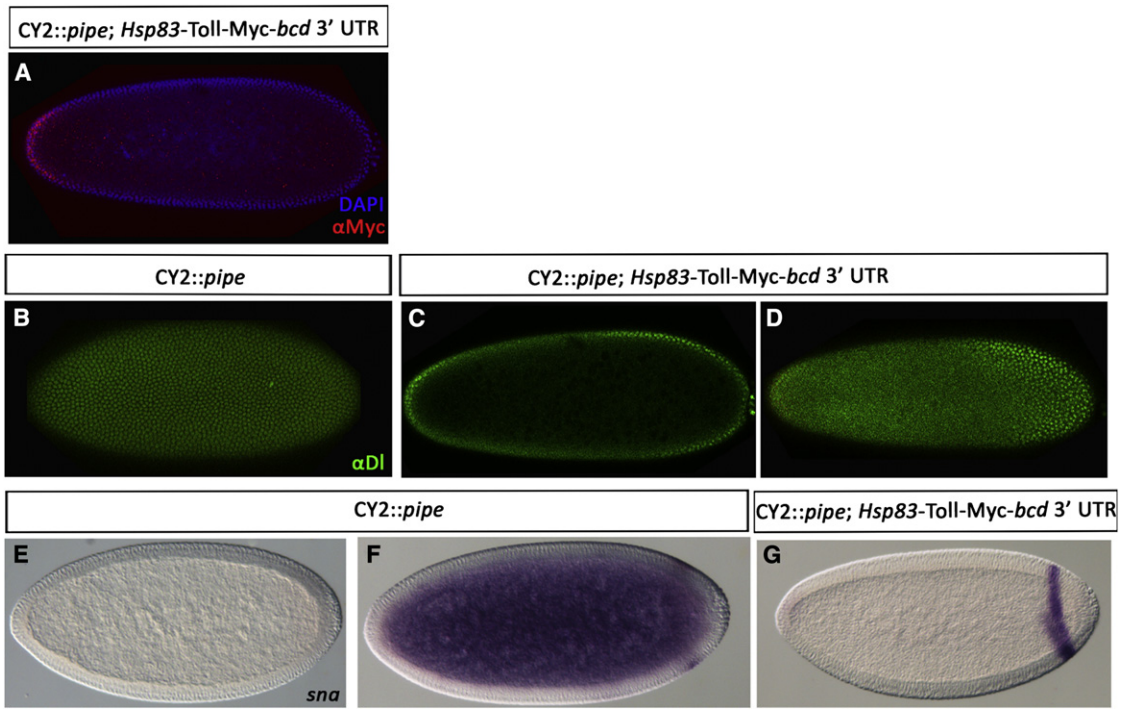

Figure 7. Anterior Tl Overexpression Leads to Short-Range Inhibition and Long-Range Activation of Dl along the AP Axis

(A) High levels of anterior Tl expression were obtained by *Hsp83* promoter and *bcd* 3′ UTR. Tl-Myc is localized to the anterior pole.

(B) Embryos laid by females expressing uniform *pipe* show uniform intermediate levels of nuclear Dl.

(C and D) Uniform *pipe* embryos that overexpress Tl at the anterior pole show short-range inhibition, indicated by low levels of nuclear Dl at the anterior region, and long-range activation, indicated by high levels at the posterior pole. High nuclear Dl at the anterior Tl overexpression domain reflects a cell-autonomous effect. Panels represent different focal planes of the same embryo.

(E) Of uniform *pipe* embryos, 81% does not express the ventral gene *sna*.

(F) Of uniform *pipe* embryos, 6% expresses *sna* in a weak posterior stripe (n = 115).

(G) Of uniform *pipe* embryos that overexpress Tl at the anterior pole, 59% expresses *sna* (n = 96), and half of them expresses *sna* in a posterior stripe. Expression of *sna* at the posterior pole indicates long-range activation, consistent with posterior shuttling of C-Spz by the anterior source of N-Spz. Anterior is oriented toward the left, and dorsal is up.

See also Figure S4.

of a patterning event taking place later in embryogenesis—the formation of the embryonic BMP activation gradient (Eldar et al., 2002; Matsuda and Shimmi, 2012; Meinhardt and Roth, 2002; Mizutani et al., 2005; Shimmi et al., 2005; Wang and Ferguson, 2005). In this context, however, the key asymmetry is provided by a prepattern that allows for asymmetric secretion of the inhibitor Sog, outside the domain being patterned, to drive the process. Such asymmetry, however, is not available to the earlier patterning system, the initial establishment of DV polarity, where the inhibitor is coproduced during morphogen processing. Our main finding is that such asymmetry is also established here, through a self-organized mechanism.

Versatile Activities of the Spz Prodomain

Self-organization is made possible by the remarkable structural and functional versatility of the N- and C-terminal domains of Spz following its cleavage by the protease Ea, and their capacity to generate an active complex, as well as an inactive complex following reassociation. Spz encodes a secreted protein that contains a signal peptide, an N-terminal prodomain, and a cysteine-rich C-terminal domain that mediates binding to the Tl receptor. An Ea cleavage site separates between these two domains. Spz is secreted as a dimer and facilitates the corresponding dimerization of Tl upon binding. However, the N terminus appears to be much more than an inhibitory prodomain. Upon cleavage by Ea the conformation of Spz is altered such that the C terminus is now exposed to bind Tl, while a noncovalent association with the N terminus is maintained. Binding to Tl releases the N-terminal region of Spz. Our model also requires the dissociation constant between Tl and C-Spz to be relatively high, allowing for release of some of the C-Spz molecules.

A central prediction of the model is that N-Spz and C-Spz can reassociate following their initial separation, and we verified this prediction experimentally. There are biological precedents for reassociation between the active ligand and its prodomain that have important physiological consequences: the BMP family ligands Myostatin and GDF11 are expressed as a proligand. In both cases, cleavage is followed by reassociation of the N-terminal prodomain with the C-terminal dimer, maintaining the ligand in a latent form. Subsequent cleavage of the prodomain by the Tolloid metalloprotease activates the latent ligand (Ge et al., 2005; Wolfman et al., 2003).

We have further demonstrated that reassociation of the N- and C-terminal domains of Spz produces a distinct form that cannot activate Tl. This diversity of Spz-based molecules thus allows the implementation of a shuttling mechanism during the early phase of development, despite the limited number of players, because each of the Spz forms plays a different role in the process. Interestingly, a distinct role for the N-terminal region of the protease Gd was recently reported. Following cleavage of this fragment, it binds the vitelline membrane in the domain defined by expression of *pipe*, and facilitates the processing of Ea by Snk (Cho et al., 2012).

The capacity of N- and C-Spz to reassociate and form an inert complex constitutes the shuttling pair. In analogy to shuttling of Dpp in the dorsal ectoderm, N-Spz fulfills an equivalent role to Sog. Indeed, we can dictate the polarity of the DV axis in lateralized embryos simply by generating a local source for producing higher levels of N-Spz that will lead to a flux, and direct the expression of mesodermal genes at the opposite pole.

In conclusion, by combining computational and experimental analyses of the Spz/Tl pathway, we demonstrate that a sharp and robust patterning gradient can be generated within a uniform region, through a mechanism we term self-organized shuttling. This mechanism relies on diverse interactions between the ligand and its prodomain, leading to a dynamic and predictable distribution of the active ligand. Although the initial shuttling models were restricted to BMP family ligands in several organisms, the current work extends the concept to another signaling pathway involving Spz and Tl. Shuttling mechanisms that generate sharp gradients are essential in the early embryo, where the spatial refinement of gene expression is minimal, and the initial patterning that takes place, prior to the onset of zygotic gene expression, cannot rely on transcriptional networks.

EXPERIMENTAL PROCEDURES

Fly Strains

The following lines were used: *UAS-pipeST2* (Sen et al., 1998), Dl-GFP (DeLotto et al., 2007), *UAS-C-Spz-GFP* inserted on a chromosome that contains a deficiency that covers *Tl* (Cho et al., 2010). *UAS–N–Spz* contains the Spz signal peptide (aa 1-29), followed by a triple V5 tag, and N-Spz (aa 30-147). It was inserted into an AttB UASp plasmid and targeted in flies into the attP40 site. *Hsp83-Tl-Myc-bcd* flies were prepared from a construct that was generated by inserting *Hsp83* promoter upstream to Tl-Myc (from T. Ip) into a pAttB plasmid. Transgenic lines were inserted into the attP40 site.

In Situ Hybridization

Probes for *ind*, *sna*, *dpp*, *sog*, and *rho* were prepared using Roche PCR Dig Probe Synthesis Kit. A probe for *pipe* was prepared using digoxigenin-labeled antisense RNA. Fixation, hybridization, and detection were as previously described by Melen et al. (2005).

DNA Constructs

N-Spz was prepared by GeneScript from a sequence of Spz signal peptide (Spz amino acids 1–29) followed by triple V5 tag, N-spz (Spz amino acids 30–147), Egfr TM domain (EGFR amino acids 803–856), followed by an HA tag. Signal peptide-C-Spz tagged with GFP (Cho et al., 2010), and Signal peptide-GFP (Schlesinger et al., 2004).

Cell Culture

HeLa cells were transfected with a DNA construct containing CMV promoter-V5-N-Spz-TM, using jutPEI (from Polyplus). S2 cells were transfected with DNA using ESCORT IV transfection reagent. Expression of *UAS-C-Spz-GFP* was achieved by cotransfection with an *actin-GAL4* plasmid. Medium of C-Spz-GFP-expressing cells was changed to fresh medium w/o serum after 1 day, collected after 2 days, and added to HeLa cells with 0.1% azide. Following 45 min incubation at 37°C, cells were washed three times with PBS and fixed at 4% FA. Antibodies used included anti-V5 (mouse, 1:800; Invitrogen) and anti-GFP (chicken, 1:1,000; Abcam).

Cuticle Preparation

Embryos were dechorionated using 6% sodium hypochlorite, and the vitelline membrane was removed using methanol (together with Heptan). Embryos were incubated in Hoyer's solution overnight at 67°C and viewed by dark-field microscopy.

Embryo Immunohistochemistry

Embryos were processed and stained as described by Ben-Yaacov et al. (2001). Primary antibodies and dilutions used in this study include anti-Vnd and anti-Msh (rat, 1:500; a gift from Z. Paroush), anti-GFP (chicken, 1:1000; Abcam), anti-Myc (mouse, 1:100; Santa-Cruz Biotechnology), and anti-Dl (mouse,1:25; Developmental Studies Hybridoma Bank). Secondary Cy2, Cy3 (Jackson ImmunoResearch), or Alexa 488, Alexa 555 (Molecular Probes) conjugated antibodies against the relevant species were used.

Cross-sections were generated using a tungsten needle on stained embryos. Images were obtained using a Zeiss LSM710 confocal system.

Numerical Screen

The following eight equations were solved systematically using MATLAB:

$$(a)\ \frac{\partial[NCSpz]}{\partial t} = D_{NC}\nabla^2[NCSpz] + \eta(x) - K_{On}[Tl][NCSpz] + K_{Off}[NCSpz - Tl] - \alpha_{NC}[NCSpz];\ \eta(x) = \eta_0\theta(L_V - |x|)$$

$$(b)\ \frac{\partial[CSpz]}{\partial t} = D_C\nabla^2[CSpz] - k_{bind}[NSpz][CSpz] + \lambda[NCSpz^*] - k_{on,C}[Tl][CSpz] + k_{off,C}[CSpz - Tl] + k_{split}[NCSpz - Tl] - \alpha_C[CSpz]$$

$$(c)\ \frac{\partial[NSpz]}{\partial t} = D_N\nabla^2[NSpz] - k_{bind}[NSpz][CSpz] + 2k_{split}[NCSpz - Tl] - \alpha_N[NSpz]$$

$$(d)\ \frac{\partial[NCSpz^*]}{\partial t} = D_{NC^*}\nabla^2[NCSpz^*] + k_{bind}[NSpz][CSpz] - \lambda[NCSpz^*]$$

$$(e)\ \frac{\partial[CSpz - Tl]}{\partial t} = k_{on,C}[Tl][CSpz] - k_{off,C}[CSpz - Tl] + k_{split}[NCSpz - Tl] - k_{end}[CSpz - Tl]$$

$$(f)\ \frac{\partial[NCSpz - Tl]}{\partial t} = K_{On}[Tl][NCSpz] - (K_{Off} + k_{split} + k_{end})[NCSpz - Tl]$$

$$(g)\ \frac{\partial[Tl_{end}]}{\partial t} = k_{end}([NCSpz - Tl] + [CSpz - Tl]) - k_{rec}[Tl_{end}]$$

$$(h)\ T^{tot} = [Tl] + [CSpz - Tl] + [NCSpz - Tl] + [Tl_{end}]$$

A total of 12 parameters were allowed to vary over several orders of magnitude, resulting in a 12-dimensional parameter space that was assayed statistically. For each such parameter set, we solved the equations in a region $-1 < x < 1$, with Spz processing occurring at $-0.4 < x < 0.4$ domain. Zero flux was assumed in the boundaries. Consistent sets were those that result in a monotonous gradient along the DV axis in which signaling in the ventral midline is at least 50% of the maximum, decreases at least by 40% from the ventral midline to $x = 0.2$, and by at least 75% to $x = 0.8$. Robustness was assessed by perturbing the production and degradation rates of all components and measuring the positions where four thresholds were met, resulting in five expression domains. A set was considered robust and consistent if at least 67% of the perturbed sets did not display a large change in expression domains, and were also consistent. See Extended Experimental Procedures, for more details of the screen.

SUPPLEMENTAL INFORMATION

Supplemental Information includes Extended Experimental Procedures, four figures, and five tables and can be found with this article online at http://dx.doi.org/10.1016/j.cell.2012.06.044.

ACKNOWLEDGMENTS

We thank R. DeLotto, T. Ip, Z. Paroush, and D. Stein for reagents; Y. Gilad, A. Rubinstein, and I. Koren for technical help; T. Volk for insightful suggestions; and Orit Bechar, Tali Wiesel, and Itzchak Reuven for their dedicated graphic design and animation work. We thank members of our groups for fruitful discussions. D.B.-Z. is supported by the Adams Fellowship Program of the Israeli Academy of Sciences and Humanities. This work was supported by the European Research Council, Israel Science Foundation, Minerva, and the Helen and Martin Kimmel Award for Innovative Investigations to N.B., who is the incumbent of the Lorna Greenberg Scherzer Professorial Chair, and the Minerva Foundation to B.-Z.S., who is an incumbent of the Hilda and Cecil Lewis Professorial Chair in Molecular Genetics.

Received: October 20, 2010
Revised: February 28, 2012
Accepted: June 19, 2012
Published: August 30, 2012

REFERENCES

Anderson, K.V. (1998). Pinning down positional information: dorsal-ventral polarity in the *Drosophila* embryo. Cell *95*, 439–442.

Ben-Yaacov, S., Le Borgne, R., Abramson, I., Schweisguth, F., and Schejter, E.D. (2001). Wasp, the *Drosophila* Wiskott-Aldrich syndrome gene homologue, is required for cell fate decisions mediated by Notch signaling. J. Cell Biol. *152*, 1–13.

Ben-Zvi, D., Shilo, B.Z., Fainsod, A., and Barkai, N. (2008). Scaling of the BMP activation gradient in *Xenopus* embryos. Nature *453*, 1205–1211.

Bier, E., Jan, L.Y., and Jan, Y.N. (1990). rhomboid, a gene required for dorsoventral axis establishment and peripheral nervous system development in *Drosophila melanogaster*. Genes Dev. *4*, 190–203.

Bollenbach, T., Kruse, K., Pantazis, P., Gonzalez-Gaitan, M., and Julicher, F. (2005). Robust formation of morphogen gradients. Phys. Rev. Lett. *94*, 18103.

Cadigan, K.M. (2002). Regulating morphogen gradients in the *Drosophila* wing. Semin. Cell Dev. Biol. *13*, 83–90.

Cho, Y.S., Stevens, L.M., and Stein, D. (2010). Pipe-dependent ventral processing of Easter by Snake is the defining step in *Drosophila* embryo DV axis formation. Curr. Biol. *20*, 1133–1137.

Cho, Y.S., Stevens, L.M., Sieverman, K.J., Nguyen, J., and Stein, D. (2012). A ventrally localized protease in the *Drosophila* egg controls embryo dorsoventral polarity. Curr. Biol. *22*, 1013–1018.

Chu, H., Parras, C., White, K., and Jiménez, F. (1998). Formation and specification of ventral neuroblasts is controlled by vnd in *Drosophila* neurogenesis. Genes Dev. *12*, 3613–3624.

DeLotto, R., DeLotto, Y., Steward, R., and Lippincott-Schwartz, J. (2007). Nucleocytoplasmic shuttling mediates the dynamic maintenance of nuclear Dorsal levels during *Drosophila* embryogenesis. Development *134*, 4233–4241.

DeLotto, Y., and DeLotto, R. (1998). Proteolytic processing of the *Drosophila* Spätzle protein by easter generates a dimeric NGF-like molecule with ventralising activity. Mech. Dev. *72*, 141–148.

DeLotto, Y., Smith, C., and DeLotto, R. (2001). Multiple isoforms of the *Drosophila* Spätzle protein are encoded by alternatively spliced maternal mRNAs in the precellular blastoderm embryo. Mol. Gen. Genet. *264*, 643–652.

Driever, W., and Nüsslein-Volhard, C. (1988a). The bicoid protein determines position in the *Drosophila* embryo in a concentration-dependent manner. Cell *54*, 95–104.

Driever, W., and Nüsslein-Volhard, C. (1988b). A gradient of bicoid protein in *Drosophila* embryos. Cell *54*, 83–93.

Eldar, A., Dorfman, R., Weiss, D., Ashe, H., Shilo, B.Z., and Barkai, N. (2002). Robustness of the BMP morphogen gradient in *Drosophila* embryonic patterning. Nature *419*, 304–308.

Eldar, A., Rosin, D., Shilo, B.Z., and Barkai, N. (2003). Self-enhanced ligand degradation underlies robustness of morphogen gradients. Dev. Cell *5*, 635–646.

Ephrussi, A., and St Johnston, D. (2004). Seeing is believing: the bicoid morphogen gradient matures. Cell *116*, 143–152.

Ge, G., Hopkins, D.R., Ho, W.B., and Greenspan, D.S. (2005). GDF11 forms a bone morphogenetic protein 1-activated latent complex that can modulate nerve growth factor-induced differentiation of PC12 cells. Mol. Cell. Biol. *25*, 5846–5858.

Huang, A.M., Rusch, J., and Levine, M. (1997). An anteroposterior Dorsal gradient in the *Drosophila* embryo. Genes Dev. *11*, 1963–1973.

James, K.E., Dorman, J.B., and Berg, C.A. (2002). Mosaic analyses reveal the function of *Drosophila* Ras in embryonic dorsoventral patterning and dorsal follicle cell morphogenesis. Development *129*, 2209–2222.

Kanodia, J.S., Rikhy, R., Kim, Y., Lund, V.K., DeLotto, R., Lippincott-Schwartz, J., and Shvartsman, S.Y. (2009). Dynamics of the Dorsal morphogen gradient. Proc. Natl. Acad. Sci. USA *106*, 21707–21712.

Lecuit, T., Brook, W.J., Ng, M., Calleja, M., Sun, H., and Cohen, S.M. (1996). Two distinct mechanisms for long-range patterning by Decapentaplegic in the *Drosophila* wing. Nature *381*, 387–393.

LeMosy, E.K., Hong, C.C., and Hashimoto, C. (1999). Signal transduction by a protease cascade. Trends Cell Biol. *9*, 102–107.

Liberman, L.M., Reeves, G.T., and Stathopoulos, A. (2009). Quantitative imaging of the Dorsal nuclear gradient reveals limitations to threshold-dependent patterning in *Drosophila*. Proc. Natl. Acad. Sci. USA *106*, 22317–22322.

Lund, V.K., DeLotto, Y., and DeLotto, R. (2010). Endocytosis is required for Toll signaling and shaping of the Dorsal/NF-kappaB morphogen gradient during *Drosophila* embryogenesis. Proc. Natl. Acad. Sci. USA *107*, 18028–18033.

Matsuda, S., and Shimmi, O. (2012). Directional transport and active retention of Dpp/BMP create wing vein patterns in *Drosophila*. Dev. Biol. *366*, 153–162.

McDonald, J.A., Holbrook, S., Isshiki, T., Weiss, J., Doe, C.Q., and Mellerick, D.M. (1998). Dorsoventral patterning in the *Drosophila* central nervous system: the vnd homeobox gene specifies ventral column identity. Genes Dev. *12*, 3603–3612.

Meinhardt, H., and Roth, S. (2002). Developmental biology: sharp peaks from shallow sources. Nature *419*, 261–262.

Melen, G.J., Levy, S., Barkai, N., and Shilo, B.Z. (2005). Threshold responses to morphogen gradients by zero-order ultrasensitivity. Mol. Syst. Biol., 1:2005.0028.

Mizutani, C.M., Nie, Q., Wan, F.Y., Zhang, Y.T., Vilmos, P., Sousa-Neves, R., Bier, E., Marsh, J.L., and Lander, A.D. (2005). Formation of the BMP activity gradient in the *Drosophila* embryo. Dev. Cell *8*, 915–924.

Morisato, D. (2001). Spätzle regulates the shape of the Dorsal gradient in the *Drosophila* embryo. Development *128*, 2309–2319.

Morisato, D., and Anderson, K.V. (1994). The Spätzle gene encodes a component of the extracellular singnaling pathway establishing the dorso-ventral pattern of the *Drosophila* embryo. Cell *76*, 677–688.

Morisato, D., and Anderson, K.V. (1995). Signaling pathways that establish the dorsal-ventral pattern of the *Drosophila* embryo. Annu. Rev. Genet. *29*, 371–399.

Moussian, B., and Roth, S. (2005). Dorsoventral axis formation in the *Drosophila* embryo—shaping and transducing a morphogen gradient. Curr. Biol. *15*, R887–R899.

Nellen, D., Burke, R., Struhl, G., and Basler, K. (1996). Direct and long-range action of a DPP morphogen gradient. Cell *85*, 357–368.

Paulsen, M., Legewie, S., Eils, R., Karaulanov, E., and Niehrs, C. (2011). Negative feedback in the bone morphogenetic protein 4 (BMP4) synexpression

group governs its dynamic signaling range and canalizes development. Proc. Natl. Acad. Sci. USA *108*, 10202–10207.

Peri, F., Technau, M., and Roth, S. (2002). Mechanisms of Gurken-dependent pipe regulation and the robustness of dorsoventral patterning in *Drosophila*. Development *129*, 2965–2975.

Plouhinec, J.L., Zakin, L., and De Robertis, E.M. (2011). Systems control of BMP morphogen flow in vertebrate embryos. Curr. Opin. Genet. Dev. *21*, 696–703.

Reeves, G.T., Trisnadi, N., Truong, T.V., Nahmad, M., Katz, S., and Stathopoulos, A. (2012). Dorsal-ventral gene expression in the *Drosophila* embryo reflects the dynamics and precision of the dorsal nuclear gradient. Dev. Cell *22*, 544–557.

Roth, S., and Schüpbach, T. (1994). The relationship between ovarian and embryonic dorsoventral patterning in *Drosophila*. Development *120*, 2245–2257.

Roth, S., Stein, D., and Nüsslein-Volhard, C. (1989). A gradient of nuclear localization of the dorsal protein determines dorsoventral pattern in the *Drosophila* embryo. Cell *59*, 1189–1202.

Rusch, J., and Levine, M. (1996). Threshold responses to the dorsal regulatory gradient and the subdivision of primary tissue territories in the *Drosophila* embryo. Curr. Opin. Genet. Dev. *6*, 416–423.

Rushlow, C.A., Han, K., Manley, J.L., and Levine, M. (1989). The graded distribution of the dorsal morphogen is initiated by selective nuclear transport in *Drosophila*. Cell *59*, 1165–1177.

Schier, A.F. (2009). Nodal morphogens. Cold Spring Harb. Perspect. Biol. *1*, a003459.

Schlesinger, A., Kiger, A., Perrimon, N., and Shilo, B.Z. (2004). Small wing PLCgamma is required for ER retention of cleaved Spitz during eye development in *Drosophila*. Dev. Cell *7*, 535–545.

Schneider, D.S., Jin, Y., Morisato, D., and Anderson, K.V. (1994). A processed form of Spätzle protein defines dorso-ventral polarity in the *Drosophila* embryo. Development *120*, 1243–1250.

Sen, J., Goltz, J.S., Stevens, L., and Stein, D. (1998). Spatially restricted expression of pipe in the *Drosophila* egg chamber defines embryonic dorsal-ventral polarity. Cell *95*, 471–481.

Shimmi, O., Umulis, D., Othmer, H., and O'Connor, M.B. (2005). Facilitated transport of a Dpp/Scw heterodimer by Sog/Tsg leads to robust patterning of the *Drosophila* blastoderm embryo. Cell *120*, 873–886.

Stathopoulos, A., and Levine, M. (2002). Linear signaling in the Toll-Dorsal pathway of *Drosophila*: activated Pelle kinase specifies all threshold outputs of gene expression while the bHLH protein Twist specifies a subset. Development *129*, 3411–3419.

Stein, D. (1995). Pattern formation: the link between ovary and embryo. Curr. Biol. *5*, 1360–1363.

Turing, A.M. (1952). The chemical basis of morphogenesis. Philos. Trans. R. Soc. Lond. B Biol. Sci. *237*, 37–72.

van der Zee, M., Stockhammer, O., von Levetzow, C., Nunes da Fonseca, R., and Roth, S. (2006). Sog/Chordin is required for ventral-to-dorsal Dpp/BMP transport and head formation in a short germ insect. Proc. Natl. Acad. Sci. USA *103*, 16307–16312.

Wang, Y.C., and Ferguson, E.L. (2005). Spatial bistability of Dpp-receptor interactions during *Drosophila* dorsal-ventral patterning. Nature *434*, 229–234.

Weber, A.N., Tauszig-Delamasure, S., Hoffmann, J.A., Lelièvre, E., Gascan, H., Ray, K.P., Morse, M.A., Imler, J.L., and Gay, N.J. (2003). Binding of the *Drosophila* cytokine Spätzle to Toll is direct and establishes signaling. Nat. Immunol. *4*, 794–800.

Weber, A.N., Gangloff, M., Moncrieffe, M.C., Hyvert, Y., Imler, J.L., and Gay, N.J. (2007). Role of the Spatzle Pro-domain in the generation of an active toll receptor ligand. J. Biol. Chem. *282*, 13522–13531.

Wolfman, N.M., McPherron, A.C., Pappano, W.N., Davies, M.V., Song, K., Tomkinson, K.N., Wright, J.F., Zhao, L., Sebald, S.M., Greenspan, D.S., and Lee, S.J. (2003). Activation of latent myostatin by the BMP-1/tolloid family of metalloproteinases. Proc. Natl. Acad. Sci. USA *100*, 15842–15846.

Wolpert, L. (1989). Positional information revisited. Development Suppl. *107*, 3–12.

Zhang, Z., Stevens, L.M., and Stein, D. (2009). Sulfation of eggshell components by Pipe defines dorsal-ventral polarity in the *Drosophila* embryo. Curr. Biol. *19*, 1200–1205.

Zhao, G., Wheeler, S.R., and Skeath, J.B. (2007). Genetic control of dorsoventral patterning and neuroblast specification in the *Drosophila* central nervous system. Int. J. Dev. Biol. *51*, 107–115.

Zhu, X., Stevens, L.M., and Stein, D. (2007). Synthesis of the sulfate donor PAPS in either the *Drosophila* germline or somatic follicle cells can support embryonic dorsal-ventral axis formation. Development *134*, 1465–1469.